

Pressure-induced development of bonding in NiAs type compounds and polymorphism of NiP

Przemyslaw Dera ^{a,*}, John D. Lazarz ^a, Barbara Lavina ^b

^a Center for Advanced Radiation Sources, The University of Chicago, Argonne National Laboratory, Building 434A 9700 South Cass Ave, Argonne, IL 60439, USA

^b High Pressure Science and Engineering Center and Department of Physics and Astronomy, University of Nevada, Las Vegas, NV 89154, USA

ARTICLE INFO

Article history:

Received 19 April 2011

Received in revised form

25 May 2011

Accepted 29 May 2011

Available online 12 June 2011

Keywords:

Nickel arsenide structure

NiP

High pressure

Phase transitions

Polymorphism

Bonding

ABSTRACT

A reversible, displacive, pressure-induced structural phase transition has been found to occur in nickel monophosphide NiP at approximately 3.5 GPa by means of *in situ* synchrotron single-crystal X-ray diffraction. The new phase, with Pearson symbol oC56, assumes an orthorhombic structure with $Cmc2_1$ space group and unit cell parameters $a=23.801(2)$ Å, $b=5.9238(6)$ Å, and $c=4.8479(4)$ Å at 5.79 GPa. The high-pressure phase is a superstructure of the ambient, $oP16$ phase with multiplicity of 3.5. The phosphorous sublattice gradually converts from the net of isolated P_2 dimers found in the ambient NiP, towards zig-zag polymeric P_∞ chains found in MnP-type structures. The transformation involves development of triatomic phosphorous clusters and interconnected Ni slabs with diamondoid topology. The high-pressure phase, which represents intermediate polymerization step, is a commensurately modulated superstructure of the NiAs aristotype. The phase transformation in NiP bears resemblance to the effect of successive substitution of Si or Ge in place of P found in the series of stoichiometric inhomogeneous linear structures in ternary $NiP_{1-x}Si_x$ and $NiP_{1-x}Ge_x$ systems.

© 2011 Elsevier Inc. All rights reserved.

1. Introduction

One of the most important and unique effects of pressure on the structure and properties of matter is its ability to affect bonding. By bringing atoms closer together the compressive strain energy is pumped into the system and can often overcome activation barriers for bond formation. Pressure-induced polymerization (PIP) is among the principal examples of pressure-induced bond formation. There are numerous known cases of high-pressure polymerization including amorphisation of aromatic molecular solids [1], polymorphism of sulfur [2], nitrogen [3] and oxygen [4]. PIP usually proceeds in one step and leads to an amorphous product, however, there are few cases in which well defined intermediate stages manifest themselves in polymorphic phase transitions, leading to structures with more extended bonded clusters (e.g. sequence of pressure-induced phase transitions in sulfur [2]). It has recently been postulated that PIP could be used to engineer high energy density materials for energy storage [5]. A very interesting case of PIP can occur in crystalline solids composed of two or more sublattices that mutually control each other through crystal field effect. Recently, a crystal-field controlled PIP of nitrogen in the structure of NaN_3 was reported [6].

The NiAs structure (space group $P6_3/mmc$, #194, Pearson code $hP4$) is one of the most common structure types found in binary transition metal compounds with 1:1 stoichiometry, and is usually specific to compounds with intermediate type of bonding, between ionic and intermetallic. The two components of the NiAs structure, the metal (M) and nonmetal (N) sublattices can interact with each other by forming bonded structures both within each sublattice (M–M and N–N), as well as between the two types of atoms (M–N), which leads to distortions of the ideal aristotype symmetry. The family of compounds assuming NiAs-related structures includes several hundred members. There are two principal types of distortions of NiAs structure, known as MnP structure type (Pearson code $oP8$) and NiP structure type (Pearson code $oP16$). In a 1986 paper Tremel et al. [7] discussed the relations between the $hP4$, $oP16$ and $oP8$ structures from the point of view of symmetry, bonding and density of states. One of the key differences between the three structures they emphasized is the topology of nearest-neighbor (NN) bonding interactions and the resulting electronic structure.

In the hexagonal NiAs structure all the NN distances for nonmetal are 3.268 Å, much longer than the typical bonding distance [8]. The metal sublattice is built from linear chains of interconnected Ni atoms separated by 2.513 Å at ambient pressure (for comparison, a Ni–Ni metallic bond in fcc nickel has a length of 2.493 Å [9]).

In NiP the nonmetal sublattice is commensurately modulated and distorted in response to formation of P_2 dimers with interatomic

* Corresponding author.

E-mail address: dera@cars.uchicago.edu (P. Dera).

distance of 2.429 Å [10], close to the typical P–P bond (for comparison the P–P bonding distance in black phosphorus is 2.224 Å [11]), while the shortest non-bonded P...P distance is 3.155 Å. The Ni sublattice is divided into isolated layers (there is no Ni–Ni bonding between the layers, but the layers are connected through the Ni–P bonds) with distorted and corrugated graphene-like geometry exhibiting bonding distances of 2.532 and 2.756 Å. The P_2 dimers are located at the centers of the 6-membered Ni_6 rings. The NiP layers found in NiP will be referred to as D-type layers. One unit cell of NiP contains two D-type layers. Tremel et al. [7] argued that it is unclear whether the P–P bonding or the Ni–Ni bonding is the primary factor controlling the distortion. From the point of view of Ni–P bonding, each Ni atom in NiP is coordinated by five P atoms located at an average distance of 2.288 Å and forming a distorted square pyramid.

In the MnP structure, on the other hand, extended zig-zag polymeric P_∞ chains of connected P atoms can be found. The bonding P–P distance is 2.667 Å [12]. The Mn sublattice is connected in a 3-dimensional framework with bonding distances of 2.706 and 2.814 Å, and much distorted diamondoid topology. The voids in the Mn framework have the largest opening along the [1 0 0] crystallographic direction of the MnP unit cell, and the P_∞ chains run along the [0 1 0] direction and are located at the center of the voids. MnP has a metal coordination number of 6, with average Mn–P distance of 2.359 Å. The oP8 distorted structure is much more common than the oP16 structure, and is especially important from the point of view of high-pressure polymorphism, as most of the compounds crystallizing in the hP4 structure transform to oP8 structure on compression.

At ambient pressure NiP crystallizes in space group $Pbca$ (#61), and assumes structure known from several other binary systems, including intermetallic compounds such as ZnAs, ZnSb, CdAs and CdSb. Interestingly, the intermetallic compounds with oP16 structure do not transform to the oP8 structure on compression, but instead were found to decompose into the elemental components [13].

Quite often structural transformation pathways found in p-T space can also be explored via crystal chemical routes, i.e. by studying solid solutions. However, in the case of the NiP–MnP system this approach involving cation-site substitution was not successful because of the limited miscibility and complex phase relations for intermediate compositions [12]. Recently, however, it has been demonstrated that the oP16 → oP8 transition can indeed be followed by anion-site substitution in ternary systems NiP_xGe_{1-x} , as well as NiP_xSi_{1-x} (NiGe and NiSi crystallize in the oP8 structure). The structural pathways for the transformations realized in these two systems are quite similar. In $NiSi_{1-x}P_x$ the

substitution occurs through formation of several intermediate stoichiometric compounds, with compositions $Ni_7P_5Si_2$, $Ni_5P_3Si_2$, Ni_2PSi , each of which assumes a different orthorhombic superstructure of NiP, with the same space group $Pbca$. The three compositions differ in the type of superstructure. In $Ni_7P_5Si_2$ (28 nickel atoms per unit cell) the supercell is formed from 3.5 basic unit cells of NiP [14], in $Ni_5P_3Si_2$ (40 nickel atoms per unit cell) the superstructure multiplicity is 5 [15], and in Ni_2PSi (16 nickel atoms per unit cell) the basic cell is doubled. In the NiP_xGe_{1-x} system two stoichiometric phases were found, $Ni_5P_3Ge_2$, Ni_2PGe , isostructural to their Si-containing counterparts, but in addition to them, in the composition range $0.3 < x < 0.7$, incommensurately modulated structures were reported [16,17].

Based on the crystal chemical analogy it seemed logical to expect a oP16 → oP8 transformation to occur, perhaps in successive stages, in the binary compound NiP as a function of pressure. Motivated by this hypothesis we conducted a series of in situ high-pressure synchrotron single-crystal diffraction experiments utilizing diamond anvil cell (DAC) apparatus and explored the pressure range up to 10 GPa.

2. Experimental

2.1. Sample

Two independent experiments (S1 and S2) were conducted to confirm the reproducibility of observations. In both experiments S1 and S2 synthetic sample prepared from a stoichiometric mixture of elements at high temperature was used. All of the single crystal micrograins used in our study were examined at ambient pressure with synchrotron single-crystal X-ray diffraction prior to high-pressure experiments, and were found to be composed of just one phase, with primitive orthorhombic unit cell $a=6.047(1)$ Å, $b=4.886(1)$ Å, $c=6.893(3)$ Å, in very good agreement with literature data for pure stoichiometric NiP: $a=6.050$ Å, $b=4.881$ Å, $c=6.890$ Å [10].

2.2. Pressure generation and X-ray diffraction data collection

In both experiments S1 and S2 multiple crystals with different orientations with respect to the DAC axis were loaded into the diamond anvil cell (two crystals in S1 and three crystals in S2). The results of both experiments are consistent with each other and confirm the occurrence of a pressure-induced structural phase transition at approximately 3.5 GPa.

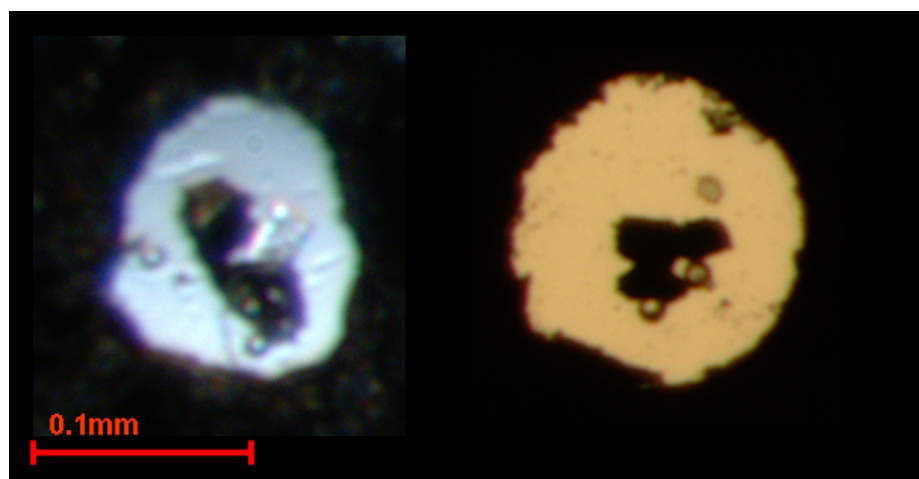


Fig. 1. Single-crystal samples of NiP loaded in Ne in experiments S1 (left) and S2 (right). In experiment S1 the NiP crystals sit on top of very thin (~3 μm) MgO slabs.

In both experiments a symmetric piston-cylinder Princeton type diamond anvil cell was used. Diamond anvils with culets of 0.3 mm were mounted on asymmetric backing plates (cubic boron nitride towards the X-ray source and tungsten carbide towards the detector). Rhenium metal gaskets preindented to 0.047 mm (experiment S_1) and 0.041 mm (experiment S_2), were used for sample containments. The DACs were loaded with neon pressure medium using the GSECARS/COMPRES gas loading system [18]. Micrographs of the samples used in each experiment are shown in Fig. 1. In both experiments pressure was estimated based on a ruby fluorescence spectrum collected at each pressure point [19]. In experiment S_1 the pressure inside the DAC after gas loading was 2.8 GPa. Single-crystal X-ray diffraction data were collected at the experimental station 13IDD of the GSECARS facility at Advanced Photon Source, Argonne National Laboratory. Monochromatic beam with incident energy of 37 keV, focused with a pair of Kirkpatrick-Baez mirrors to a spot of 0.003 by 0.005 mm was used. Diffraction images were collected using MAR165 charge coupled device (CCD) detector, placed at a sample-to detector distance of approximately 200 mm. During the exposure the sample was rotated about the vertical axis of the instrument (ω) in the range of $\pm 13^\circ$ in experiment S_1 and $\pm 25^\circ$ in experiment S_2 (in this case Boehler-Almax geometry anvil and backing plate were used on the detector side to increase angular access to the sample), with a typical exposure time of 0.5 s/deg. Diffraction images were collected at three different detector positions, differing by a translation by 70 mm perpendicular to the incident beam. The detector geometry parameters at each detector position were calibrated with CeO_2 diffraction standard. In addition to the full-rotation exposures, a step-scan with 1° rotation steps was performed at each pressure step, for each of the sample crystals. Diffraction images were analyzed using the GSE_ADA/RSV software package [20].

Diffraction data collected during experiment S_1 at the first pressure point (Fig. 2a) could be successfully indexed using the orthorhombic unit cell of the ambient pressure phase (oP16). On the first pressure increase, to 6.55 GPa new diffraction peaks appeared, as shown in Fig. 1b. Diffraction patterns collected from

both sample crystals showed consistently the same effect. The new patterns were indexed *ab initio* (without making any initial assumptions about the unit cell) and yielded a large C-centered orthorhombic unit cell, with $a=23.774(2)$ Å, $b=5.9143(6)$ Å and $c=4.8396(4)$ Å. Subsequent analysis of systematic absences indicated the most likely space group to be $Cmc2_1$ (#36). The unit cell of the new phase is closely related to that of the original oP16 phase, with the c parameter multiplied 3.5 times (the unit cell parameters of the high and low pressure phase are related as: $a_h=3.5c_l$, $b_h=a_l$, $c_h=b_l$, where indices h and l correspond to the oC56 and oP16 phases, respectively) and contains 28 formula units of NiP (Pearson code oC56). In order to verify reversibility of the transition and to better constrain the value of pressure at which it occurs, the pressure was lowered to 3.6 GPa. The diffraction pattern at 3.6 GPa still indicated the oC56 structure. On further pressure decrease to 1.29 GPa the sample converted back to the original oP16 phase. The transformation could be repeated several times without any loss of crystal quality.

In order to reconfirm the observation made during experiment S_1 , we loaded another DAC with three new crystals of NiP. All of the samples in experiment S_2 went through exactly the same phase transition as in experiment S_1 .

2.3. Structure solution and refinement

The structure of the oC56 high-pressure phases of NiP is new and different from the known structures of the phases found in the ternary $\text{NiP}_x\text{Ge}_{1-x}$ and $\text{NiP}_x\text{Si}_{1-x}$ systems, or any other systems, therefore, it was necessary to perform full *ab initio* structure determination. For that purpose integrated peak intensities collected in experiment S_2 at 5.79 GPa were fitted using the GSE_ADA program, and corrected for DAC absorption, Lorenz and polarization effects. Because of the high incident energy and negligible sample thickness the sample absorption was ignored. Peaks from exposures at the three different detector positions were scaled and merged together. The resulting lists of peaks with corresponding squares of structure factor amplitudes $|F|^2$ and their standard deviations were used for structure solution and

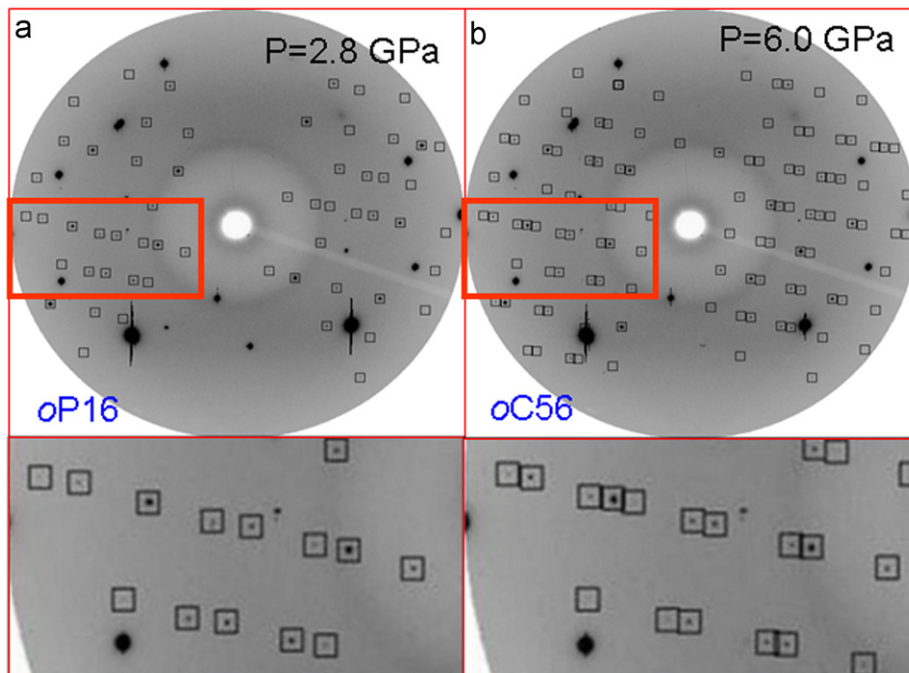


Fig. 2. Evolution of single-crystal diffraction pattern of NiP with pressure in experiments S_1 . A new phase transition occurring at approximately 3.5 GPa is indicated by appearance of new families of diffraction peaks.

Table 1

Crystallographic information for structure refinements of the oP16 and oC56 phases of NiP.

Empirical formula	NiP	
Temperature	293(2) K	
Pressure	1.29 GPa	5.79 GPa
Wavelength	0.33440 Å	
Crystal system, space group	Orthorhombic, <i>Pbca</i> (no. 61)	Orthorhombic, <i>Cmc2</i> ₁ (no. 36)
Pearson symbol	oP16	oC56
Unit cell dimensions	<i>a</i> =6.0360(4) Å <i>b</i> =4.8684(2) Å <i>c</i> =6.8788(4) Å <i>V</i> =202.13(2) Å ³ 8, 5.892 g/cm ³ 2.89 to 18.14 deg.	<i>a</i> =23.801(2) Å <i>b</i> =5.9238(6) Å <i>c</i> =4.8479(4) Å <i>V</i> =683.53(9) Å ³ 28, 6.099 g/cm ³ 1.67 to 18.06 deg.
Z, Calculated density		
Theta range for data collection	2.89 to 18.14 deg.	-20 < <i>h</i> < 15, -9 < <i>k</i> < 9, -7 < <i>l</i> < 7
Limiting indices	-9 < <i>h</i> < 9, -7 < <i>k</i> < 7, -5 < <i>l</i> < 4	897/471 [R(int)=0.0892]
Reflections collected / unique	465/165 [R(int)=0.0986]	23.2%
Completeness to theta=18.1	24.2%	
Refinement method	Full-matrix least-squares on <i>F</i> ²	
Data/restraints/parameters	165/0/19	471/1/67
Goodness-of-fit on <i>F</i> ²	1.112	1.084
Final R indices [<i>I</i> > 2sigma(<i>I</i>)]	<i>R</i> 1=0.0432, <i>wR</i> 2=0.1073	<i>R</i> 1=0.0494, <i>wR</i> 2=0.1077
R indices (all data)	<i>R</i> 1=0.0440, <i>wR</i> 2=0.1075	<i>R</i> 1=0.0494, <i>wR</i> 2=0.1077
Largest diff. peak and hole	1.325 and -1.203 e/Å ³	1.371 and -1.453 e/Å ³

subsequent refinement. A total of 897 reflections (471 unique) have been found in the three wide oscillation diffraction images collected. The structure was solved by means of simulated annealing approach, as implemented in the computer program Endeavour [21,22]. For structure solution the starting model for the oC56 phase was derived by taking the fractional atomic coordinates of the atoms in the oP16 phase unit cell (symmetry reduced to *P*1) and repeating them to fill up the oC56 unit cell. The resulting model was locally refined using the simulated annealing method, by minimizing the difference between the calculated and observed diffraction patterns, and at the same time minimizing the energy of interatomic interactions as approximated by means of simple repulsion potentials with cost function set at 0.3. The local refinement quickly converged to a solution with *R*-factor of ~12%. The resulting model was then used as a starting point for a conventional least squares crystal structure refinement using the SHELXL program [23], which converged to *R*1=4.94%. Structure refinement was done using anisotropic displacement parameters for all atoms.

For comparison of the structures of the two phases we also performed high-pressure structure refinement of the ambient oP16 phase at 1.29 GPa. The data analysis was performed analogically as for the oC56 phase, except that the structure solution was not necessary. The crystallographic parameters for the two final structure determinations are summarized in Table 1. Fractional atomic coordinates for the oP16 and oC56 models are listed in Table 2. Anisotropic displacement parameters are listed in Table 3.

3. Discussion

3.1. The mechanism of the oP16→oC56 transition

The high-pressure transformation occurs at approximately 3.5 GPa, is fully reversible, and involves almost no hysteresis. The high-pressure superstructure assumes space group *Cmc2*₁, which is often encountered in the NiAs structural family [24]. In the crystal structure of the oC56 phase there are four symmetry independent Ni atoms, and four P atoms. The structures of the oP16, oC56 and oP8 phases are compared in Fig. 3.

Due to the displacive character of the oP16→oC56 transition the arrangement of atoms in the high-pressure phase does not change

Table 2

Fractional atomic coordinates ($\times 10^4$) and equivalent isotropic displacement parameters ($\text{\AA}^2 \times 10^3$) for the oP16 phase at 1.29 GPa and oC56 phase at 5.79 GPa. $U(eq)$ is defined as one-third of the trace of the orthogonalized U_{ij} tensor.

Atom name	x	y	z	$U(eq)$
NiP in oP16 phase at 1.29 GPa				
Ni(1)	1945(1)	117(2)	3968(3)	8(1)
P(1)	589(3)	1744(4)	1127(5)	10(1)
NiP in oC56 phase at 5.79 GPa				
Ni(1)	4368(1)	496(3)	4200(3)	9(1)
Ni(2)	1477(1)	552(4)	4066(4)	7(1)
Ni(3)	2071(1)	4438(4)	3842(3)	8(1)
Ni(4)	0	518(5)	8991(5)	8(2)
P(1)	4306(4)	3187(5)	991(8)	8(2)
P(2)	1444(3)	3094(6)	706(11)	8(3)
P(3)	2894(4)	3120(7)	2200(12)	8(3)
P(4)	0	3141(9)	2362(13)	8(4)

Table 3

Anisotropic displacement parameters ($\text{\AA}^2 \times 10^3$) for the oP16 phase at 1.29 GPa and oC56 phase at 5.79 GPa. The anisotropic displacement factor exponent takes the form: $-2pi^2[h^2 a^{*2} U11 + \dots + 2hka^*b^*U12]$.

Atom name	<i>U</i> 11	<i>U</i> 22	<i>U</i> 33	<i>U</i> 23	<i>U</i> 13	<i>U</i> 12
NiP in oP16 phase at 1.29 GPa						
Ni(1)	8(1)	7(1)	9(2)	1(1)	-1(1)	0(1)
P(1)	7(1)	9(1)	14(4)	3(1)	1(1)	0(1)
NiP in oC56 phase at 5.79 GPa						
Ni(1)	11(3)	10(1)	5(1)	0(1)	1(1)	1(1)
Ni(2)	6(4)	7(1)	8(1)	2(1)	2(1)	0(1)
Ni(3)	8(4)	8(1)	8(1)	-1(1)	0(1)	3(1)
Ni(4)	10(5)	8(1)	6(1)	3(1)	0	0
P(1)	3(8)	8(1)	13(2)	1(1)	-5(3)	-2(2)
P(2)	9(10)	5(2)	9(2)	0(1)	-1(2)	-1(2)
P(3)	7(10)	8(2)	7(1)	-3(1)	-3(3)	0(2)
P(4)	9(13)	9(2)	5(2)	-4(2)	0	0

significantly. Within the structure one can still distinguish separate layers of interconnected Ni atoms, which are now oriented perpendicular to the crystallographic [1 0 0] direction (equivalent to [0 0 1] in the primitive unit cell of the oP16 phase). In the oC56 phase every fourth of oP16-type layers is now modified through formation of P₃ trimers that replace all of the P₂ dimers from the low pressure phase

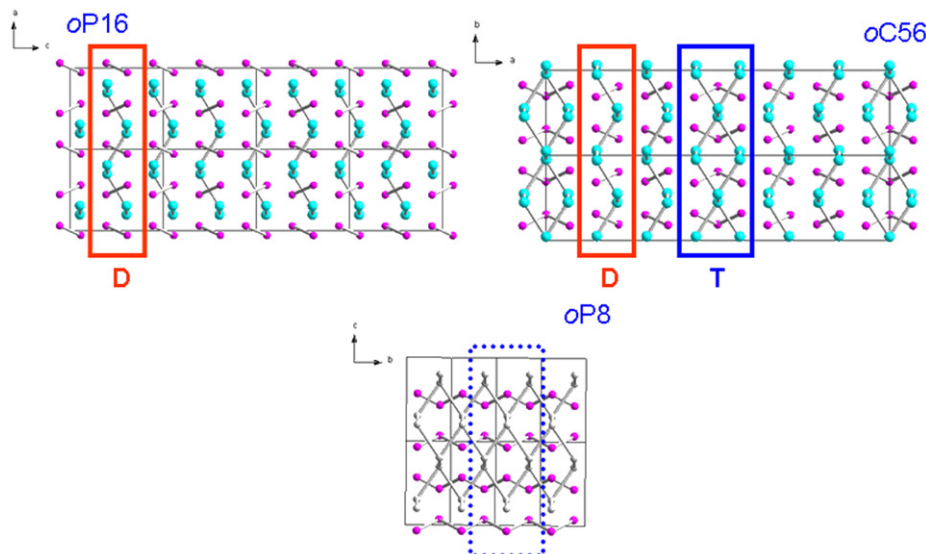


Fig. 3. Structural changes accompanying transformation from oP16 to oC56 phase. For comparison the structure of the oP8 MnP phase is also shown along the equivalent direction.

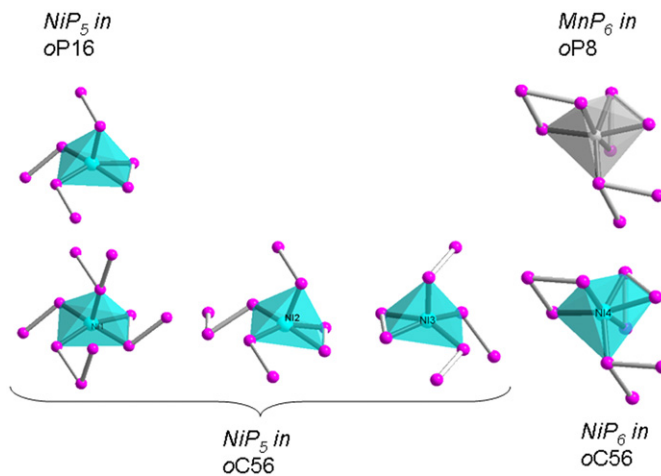


Fig. 4. Comparison of the geometry of Ni coordination polyhedral in the oP16, oC56 and oP8 phases.

(the T-layer). The P_3 units are characterized by a P–P bond length of 2.539(8) Å (the P–P bond length for the P_2 units is 2.426(6) Å) and P–P–P valence angle of 81.2(4) degrees at 5.79 GPa (the P–P–P angle in MnP is 73.0 [12]). The P atoms forming P_3 units are P1 and P4, while P2 and P3 participate in P_2 dimers only. In terms of the content of P_2 and P_3 units in the unit cell the oC56 phase can be described as $Ni_{28}(P_3)_4(P_2)_8$, while for the oP16 phase the analogous formula is $Ni_8(P_2)_4$.

The formation of P_3 trimers has two consequences: (i) the structure of the Ni part of the T-layer is modified, as it is now extended to include half of the Ni atoms from the neighboring D-layer (so if the composition of the D-layer is NiP, the composition of the T layer becomes $Ni_{1.5}P_{1.5}$) and (ii) in order to preserve the composition of the D-layers, the D-layers on one side of the trimeric layer, are now inverted with respect to their original orientation as defined by the inclination of the P_2 units and buckling pattern of the Ni substructure. The Ni atoms forming the D-layers are Ni2 and Ni3.

Ni1 atoms are the "external" atoms of the T-layer, while Ni4 are the "internal" atoms. The geometry of the D-layers remains almost unchanged and the coordination number within these layers remains 5, with average Ni–P distance of 2.289, 2.255 and

2.271 Å for Ni1, Ni2 and Ni3, respectively. The environment of the external Ni atoms of T-layers is almost the same as that of the D-layers, and the N1 atoms are also characterized by a coordination number of 5. The Ni4 atoms, on the other hand, which are located at the center of the condensed T-layer increase their coordination number to 6 (like in MnP) with average Ni–P bonding distance of 2.324 Å and geometry of very distorted octahedron. Changes in the Ni coordination environment geometry accompanying the oP16 → oC56 transition are illustrated in Fig. 4. A single unit cell of oC56 consists of two T-type layers and four D-type layers, resulting in composition of D_2T , and is 3.5 times larger than a unit cell of the oP16 phase. The geometry of the T-layers is basically identical as the geometry of similar units found in the MnP structure, except that in the latter the layers are not separated, but connected with each other through condensation of P atoms into infinite P_∞ chains. Quite clearly, the transformation is driven by the development of new bonding P–P and Ni–Ni interactions, which modulates the whole structure.

3.2. Density and molar volume evolution

In the oP16 phase the a and c unit cell parameters show exactly the same compressibility, while the b parameter exhibits a much higher pressure gradient, as shown in Fig. 5. The oP16 → oC56 transition is accompanied by approximately 1% volume decrease, and is therefore first order. All of the unit cell parameters change discontinuously at the transition point. The b unit cell parameter of the oP16 phase expands by 0.4%, whereas a and c contract by 1.1% and 0.6%, respectively. The b parameter corresponds to the direction within the layers, where the Ni_6 rings are elongated; its expansion is necessary to properly accommodate more extended phosphorous structures inside the ring voids. The change in the unit cell shape is understandable, by comparing the shapes of the equivalent NiP and MnP unit cells at ambient conditions. The MnP cell is expanded by 7.7%, with respect to the NiP cell along the oP16 b direction, and contacted by 7.9% and 2.2% along the oP16 c and a , respectively. The change in the unit cell shape is clearly a consequence of the development of the new bonds.

To the best of our knowledge the equation of state of NiP has not been studied before. Compressibility of MnP structure type compounds varies quite strongly as a function of composition. For example, for FeP $K_0=205(7)$ GPa ($K'=4$) [25], for FeS

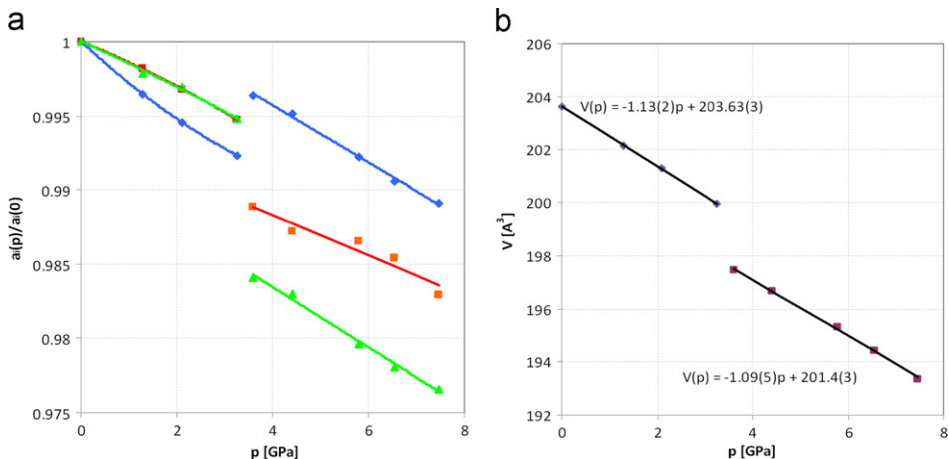


Fig. 5. Evolution of normalized unit cell parameters and volume with pressure measured in experiment S2. In the left plot diamond symbols represents b/b_0 , squares represents c/c_0 and triangles a/a_0 (all in the oP16 phase setting). The a parameter of the oC56 phase and the volume of the unit cell of oC56 phase have been scaled to the oP16 phase equivalent. The error bars are smaller than the data point symbols.

$K_0=34.8(35)$ GPa ($K'=5$) [26], and for FeAs $K_0=122.9(1)$ GPa ($K'=4$) [27], respectively. The pressure dependence of the unit cell volume for both the low as well as high-pressure phases of NiP exhibits very little curvature. From a linear fit the pressure gradient of the unit cell volume for the high-pressure phase is smaller by 3.3% than the pressure gradient of the oP16 phase, as shown in Fig. 5, which means that the higher density oC56 phase is less compressible. A fit with 3-order Birch-Murnaghan equation of state to the experimental data yields $K_0=173(2)$ GPa and $V_0=203.65(2)$ Å³ for the oP16 phase and $K_0=163(6)$ GPa and $V_0=706.2(8)$ Å³ for the oC56 phase.

3.3. Crystal chemical analogs

There are clear analogies between the pressure-induced polymorphism reported here and the sequence of stoichiometric compounds with increasing Si content in $\text{NiP}_x\text{Si}_{1-x}$. The high-pressure oC56 phase has exactly the same superstructure multiplicity as the oP56 phase of $\text{Ni}_7\text{P}_5\text{Si}_2$ structure (lowest Si concentration of the $\text{NiP}_x\text{Si}_{1-x}$ series), although the space group is different.

In general, while the structures are not exactly equivalent, the successive pressure-induced polymerization of P in the NiP structure much resembles replacement of the P atoms by Si or Ge, which is justified by the fact that Si has a smaller ionic radius than P and ionic radius decreases at high pressure. According to our observations, the transformation path through the incommensurately modulated structures found in $\text{NiP}_x\text{Ge}_{1-x}$ [16] is not realized in NiP at high pressure below 10 GPa.

From the point of view of the bonding topology, the oP16 structure constitutes an intermediate stage between the isolated atom semimetal sublattice in hP4 and zig-zag chains in oP8 structures. While the hP4 → oP8 transformation is found to occur at high pressure quite commonly, to our knowledge oP16 intermediate phase has never been observed.

Interestingly, while the hexagonal NiAs structure (space group $P6_3/mmc$, # 194) is the aristotype of the whole family of compounds, it is now believed that the mineral NiAs nickeline, after which the structure type is named, does not actually assume the ideal, archetypic symmetry itself, and instead should be properly described in orthorhombic setting, with space group $Cmc2_1$ (#36, Pearson code oC24, unit cell $a=10.857$ Å, $b=6.268$ Å, $c=5.034$ Å), exactly the same as in oC56 phase of NiP [24]. However, in NiAs at ambient conditions the magnitude of the departure from the hexagonal symmetry is negligible.

3.4. Relation to other known pressure-induced phase transitions in NiAs-related compounds

While in many cases pressure-induced hP4 → oP8 transformations proceed directly, there are also known cases of the same transformation proceeding through intermediate phases (other than oP16). For example, in MnTe the ambient hP4 phase first transforms to a phase with unknown structure at 10 GPa, and then to the oP8 structure at 24 GPa [28]. In troilite (FeS) hP4 is a high temperature phase, which can be converted to antiferromagnetic oP8 on cooling (this transition proceeds through an intermediate, 3a-2c hexagonal phase) at high-pressure, or directly to nonmagnetic oP8 above 30 GPa at high temperature [26]. Recent first principles calculations [29] predict acoustic phonon instabilities in NiAs-structured AlP and AlAs. It seems likely that some of these not yet well characterized intermediate phases can be formed through mechanisms similar to the one driving the pressure-induced polymorphism in NiP. The transformation described in this study proceeded through displacive mechanism, which did not destroy the single-crystal nature of the samples; therefore, similar expectation can be applied to other systems from NiAs family undergoing pressure-induced distortions as a result of bonding development. As a consequence, single-crystal X-ray diffraction experiments could be recommended as a promising approach to reveal the structures of the still elusive high-pressure phases.

4. Conclusions

Nickel monophosphide, NiP has been found to exhibit a previously unknown pressure-induced phase transition related to successive development of bonding and formation of P_3 trimeric structures in the phosphorous sublattice, accompanied by formation of Ni clusters with diamondoid topology. The new high-pressure oC56 phase forms at approximately 3.5 GPa through reversible, displacive phase transitions. The structure of the new phase has been determined by means of synchrotron single-crystal X-ray diffraction. The oC56 structure of NiP does not yet constitute the final stage of P polymerization; therefore further structural transformations at pressures higher than 10 GPa, leading most likely to the oP8, or closely related structure are expected.

Acknowledgments

The authors would like to thank Dr. Nabil Z. Boctor from the Geophysical Laboratory, Carnegie Institution of Washington for kindly providing synthetic NiP material and Prof. Roald Hoffmann, Cornell University, as well as three anonymous reviewers for reading the manuscript and providing very useful suggestions. This work was performed at GSECARS (Sector 13), Advanced Photon Source (APS), Argonne National Laboratory. GSECARS is supported by the NSF Grant EAR-06.22171 and DOE Geosciences Grant DE-FG02-94ER14466. Use of the Advanced Photon Source was supported by the U. S. Department of Energy, Office of Science, Office of Basic Energy Sciences, under Contract no. DE-AC02-06CH11357.

References

- [1] M. Gauthier, J.C. Chervin, P. Pruzan, *High Pressure Res.* 9 (1992) 300–304.
- [2] O. Degtyareva, et al., *Nat. Mater.* 4 (2005) 152–155.
- [3] I.A. Trojan, et al., *Appl. Phys. Lett.* 93 (2008) 091907.
- [4] L.F. Lundgaard, et al., *Nature* 443 (2006) 201–204.
- [5] M.J. Lipp, et al., *Nat. Mater.* 4 (2005) 211–215.
- [6] M.I. Eremets, et al., *J. Chem. Phys.* 120 (2004) 10618–10623.
- [7] W. Tremel, R. Hoffmann, J. Silvestre, *J. Am. Chem. Soc.* 108 (1986) 5174–5187.
- [8] R.A. Yund, *Econ. Geol. Bull. Soc.* 56 (1962) 1273–1296.
- [9] R. Diamant, *Met.: Corros. Ind.* 31 (1956) 167–187.
- [10] E. Larsson, *Ark. Kemi* 23 (1965) 335–365.
- [11] A. Brown, S. Rundqvist, *Acta Cryst.* 19 (1965) 684–685.
- [12] H. Fjellvag, A. Kjekshus, *Acta Chem. Scand.* A38 (1984) 719–724.
- [13] V.F. Degtyareva, I.K. Bdikin, S.S. Khasanov, *Phys. Solid State* 39 (1997) 1341–1344.
- [14] S.V. Oryshchyn, et al., *Zeitschr. Krist.* 214 (1999) 337–340.
- [15] O.N. Ilnitskaya, et al., *Sov. Phys. Crystallogr.* 37 (1992) 76–78.
- [16] A.K. Larsson, F.J. Garcia-Garcia, R.L. Withers, *J. Solid State Chem.* 180 (2007) 1093–1102.
- [17] F.J. Garcia-Garcia, A.K. Larsson, *J. Solid State Chem.* 178 (2007) 742–754.
- [18] M.L. Rivers, et al., *High Pressure Res.* 28 (2008) 273–292.
- [19] H.K. Mao, J. Xu, P.M. Bell, *J. Geophys. Res.* 91 (1986) 4673–4676.
- [20] P. Dera, GSE_ADA data analysis program for monochromatic single crystal diffraction with area detector, GSECARS, Chicago, IL, 2007.
- [21] Endeavour, Crystal Impact GbR <<http://www.crystalimpact.com/endeavour>>, Bonn, 2009.
- [22] H. Putz, J.C. Schon, M. Jansen, *J. Appl. Cryst.* 32 (1999) 864–870.
- [23] G.M. Sheldrick, *Acta Cryst. A64* (2008) 112–122.
- [24] J.G. Thompson, et al., *J. Phys. C: Solid State Phys.* 21 (1988) 4007–4015.
- [25] T. Gu, et al., *Phys. Earth Plan. Inter.* 184 (2011) 154–159.
- [26] H.E. King, C.T. Prewitt, *Acta Cryst. B38* (1982) 1877–1887.
- [27] P.S. Lyman, C.T. Prewitt, *Acta Cryst. B40* (1984) 14–20.
- [28] M. Mimasaka, et al., *J. Phys. C: Solid State Phys.* 20 (1987) 4689–4694.
- [29] Y. Li, et al., *Phys. Rev. B81* (2010) 052101.